EINDHOVEN UNIVERSITY OF TECHNOLOGY

Epitaxial Ge0.81Sn0.19 nanowires for nanoscale mid-infrared emitters

Citation for published version (APA):
Seifner, M. S., Dijkstra, A., Bernardi, J., Steiger-Thirsfeld, A., Sistani, M., Lugstein, A., Haverkort, J. E. M., & Barth, S. (2019). Epitaxial Ge0.81Sn0.19 nanowires for nanoscale mid-infrared emitters. *ACS Nano*, *13*(7), 8047-8054. https://doi.org/10.1021/acsnano.9b02843

Document license:
TAVERNE

DOI:
10.1021/acsnano.9b02843

Document status and date:
Published: 23/07/2019

Document Version:
Publisher's PDF, also known as Version of Record (includes final page, issue and volume numbers)

Please check the document version of this publication:

• A submitted manuscript is the version of the article upon submission and before peer-review. There can be important differences between the submitted version and the official published version of record. People interested in the research are advised to contact the author for the final version of the publication, or visit the DOI to the publisher's website.
• The final author version and the galley proof are versions of the publication after peer review.
• The final published version features the final layout of the paper including the volume, issue and page numbers.

Link to publication

General rights
Copyright and moral rights for the publications made accessible in the public portal are retained by the authors and/or other copyright owners and it is a condition of accessing publications that users recognise and abide by the legal requirements associated with these rights.

• Users may download and print one copy of any publication from the public portal for the purpose of private study or research.
• You may not further distribute the material or use it for any profit-making activity or commercial gain
• You may freely distribute the URL identifying the publication in the public portal.

If the publication is distributed under the terms of Article 25fa of the Dutch Copyright Act, indicated by the "Taverne" license above, please follow below link for the End User Agreement:

www.tue.nl/taverne

Take down policy
If you believe that this document breaches copyright please contact us at:

openaccess@tue.nl

providing details and we will investigate your claim.

Download date: 04. Oct. 2023

ACS NANO
Cite This: ACS Nano 2019, 13, 8047−8054
www.acsnano.org

ARTICLE

Epitaxial $Ge_{0.81}Sn_{0.19}$ Nanowires for Nanoscale Mid-Infrared Emitters

Michael S. Seifner,[†] Alain Dijkstra,[‡] Johannes Bernardi,[§] Andreas Steiger-Thirsfeld,[§] Masiar Sistani,[∥] Alois Lugstein,[∥] Jos E. M. Haverkort,[‡] and Sven Barth*,[†,⊥]

[†]Institute of Materials Chemistry, TU Wien, Getreidemarkt 9/BC/02, A-1060 Vienna, Austria
[‡]Department of Applied Physics, Eindhoven University of Technology, 5600MB Eindhoven, The Netherlands
[§]University Service Center for TEM (USTEM), TU Wien, Wiedner Hauptstraße 8-10, 1040 Vienna, Austria
[∥]Institute of Solid State Electronics, TU Wien, Gußhausstraße 25-25a, 1040 Vienna, Austria
[⊥]Physikalisches Institut, Goethe-Universität Frankfurt, Max-von-Laue-Straße 1, 60438 Frankfurt am Main, Germany

Supporting Information

Downloaded via TU EINDHOVEN on August 21, 2019 at 06:43:49 (UTC).
See https://pubs.acs.org/sharingguidelines for options on how to legitimately share published articles.

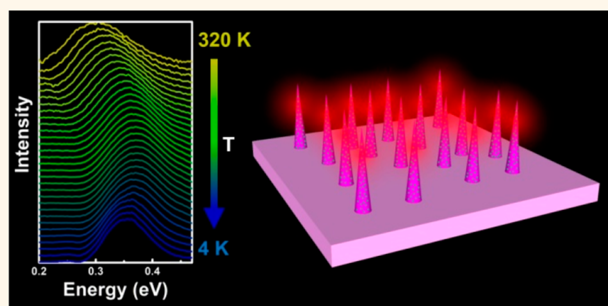

ABSTRACT: **Highly oriented $Ge_{0.81}Sn_{0.19}$ nanowires have been synthesized by a low-temperature chemical vapor deposition growth technique. The nanostructures form by a self-seeded vapor−liquid−solid mechanism. In this process, liquid metallic Sn seeds enable the anisotropic crystal growth and act as a sole source of Sn for the formation of the metastable $Ge_{1-x}Sn_x$ semiconductor material. The strain relaxation for a lattice mismatch of ε = 2.94% between the Ge (111) substrate and the constant $Ge_{0.81}Sn_{0.19}$ composition of nanowires is confined to a transition zone of <100 nm. In contrast, $Ge_{1-x}Sn_x$ structures with diameters in the micrometer range show a 5-fold longer compositional gradient very similar to epitaxial thin-film growth. Effects of the Sn growth promoters' dimensions on the morphological and compositional evolution of $Ge_{1-x}Sn_x$ are described. The temperature- and laser power-dependent photoluminescence analyses verify the formation of a direct band gap material with emission in the mid-infrared region and values expected for unstrained $Ge_{0.81}Sn_{0.19}$ (*e.g.*, band gap of 0.3 eV at room temperature). These materials hold promise in applications such as thermal imaging and photodetection as well as building blocks for group IV-based mid- to near-IR photonics.**

KEYWORDS: *semiconductor, nanowires, epitaxy, direct band gap, germanium, tin*

Monolithic integration of photonics and electronics based on all-group IV semiconductors requires a localized and efficient way of fabricating light emitters being processed in established complementary metal-oxide-semiconductor (CMOS) compatible processes.[1] For this purpose, direct band gap $Ge_{1-x}Sn_x$ has recently regained increased interest.[2,3] Alloying germanium with tin alters the characteristics of the semiconductor, tremendously affecting electronic,[4] optoelectronic,[5] and optical[6] properties. However, a direct semiconductor material of this element combination requires transcending the equilibrium solubility of ∼1 at%,[7] and compositions of ⩾8 at% Sn[8] are desired. The efficient incorporation of high Sn contents in Ge can be achieved by crystal growth under non-equilibrium conditions ruled by kinetics. These metastable $Ge_{1-x}Sn_x$ materials are candidates for infrared optoelectronics and optical devices, such as lasers,[8−12] photodetectors,[13,14] or light-emitting diodes[15−17] due to their composition-dependent direct band gaps.[18]

Despite significant progress in thin-film growth techniques, there is a limited number of reports available for anisotropic $Ge_{1-x}Sn_x$ crystal growth exceeding the Sn content needed to obtain a direct band gap material. $Ge_{1-x}Sn_x$ nanowires (NWs) have been prepared using Au growth seeds and simultaneous decomposition of allyltributylstannane and diphenylgermane leading to $Ge_{0.91}Sn_{0.09}$ with characteristics of a direct band gap material.[19,20] Higher Sn contents in the range of 17−28 at% have been obtained in anisotropic $Ge_{1-x}Sn_x$ nanostructures by applying a liquid-based approach.[21−23] The material in this composition range reveals high conductivity values and semiconductor behavior.[24]

Low-temperature growth enabling the formation of metastable phases can lead to extraordinary high doping levels in Ge NWs while retaining excellent crystal quality. For instance,

Received: April 12, 2019
Accepted: July 8, 2019
Published: July 8, 2019

© 2019 American Chemical Society

DOI: 10.1021/acsnano.9b02843
ACS Nano 2019, 13, 8047−8054

chemical vapor deposition (CVD) as well as electrochemical approaches have the potential to incorporate very high concentrations of the metal used to grow the Ge nanocrystals.[25−28] The technique applied in the aforementioned growth studies can be described as a low-temperature variation of the self-seeded growth described for In or Ga metal of the respective III−V NWs.[29,30] In this context, Sn has been used in prior studies for the growth of Si[31,32] and Ge[33,34] nanorods/NWs and segmented Si/Ge heterostructures;[35,36] however, significant incorporation from a Sn reservoir in the growing Ge NW crystal has only been achieved by low-temperature microwave-based syntheses[21−23] according to the solution-liquid−solid mechanism and for in-plane migrating NWs[37] using a solid−liquid−solid approach.

Thus far, only one study on metal-catalyzed growth of $Ge_{1-x}Sn_x$ NWs with specific orientation on substrates has been reported. Although the temperature used in the study is in the regime (300−350 °C) where efficient Sn incorporation has been demonstrated for layer growth, the Ge NWs contain only the thermodynamically stable ∼1 at% Sn and reveal a Sn−O-enriched shell.[38] A successful strategy to prepare anisotropic nanostructures has been the epitaxial growth of $Ge_{1-x}Sn_x$ shells on pre-oriented Ge NWs as a substrate material.[39,40] The most efficient incorporation in these studies shows an epitaxial, nonhomogeneous $Ge_{0.87}Sn_{0.13}$ shell growth with a significant Sn gradient of 8−13 at%.[39] The shell accommodates the strain by the aforementioned Sn gradient and also by an inhomogeneous distribution of Sn with radial "sunburst stripes" of low (∼5 at%) and high Sn content (8−13 at%) alternating segments.[41]

Here, we report an efficient CVD growth method of anisotropic $Ge_{1-x}Sn_x$ structures on Ge (111) substrates. Epitaxial, vertically grown $Ge_{1-x}Sn_x$ (x = 0.15−0.19) structures are demonstrated over a large diameter range of ∼50−1100 nm. The initial Sn particle acts as both nucleation seed as well as Sn source for the formation of the binary semiconductor, and thus the growth mechanism can be described as a self-seeding vapor-liquid-solid (VLS) mechanism. Short growth cycles have been intentionally chosen to prevent potential thermal degradation of the material, which we investigated prior to this study.[23] Our results demonstrate a diameter-dependent gradient/transition zone between substrate and $Ge_{1-x}Sn_x$ material with very efficient strain relaxation for nanostructures. The obtained $Ge_{0.81}Sn_{0.19}$ NWs exhibit photoluminescence (PL) showing a low-temperature band gap at the expected energy of 0.37 eV for unstrained material.[42] Although the effective areal $Ge_{0.81}Sn_{0.19}$ volume of the NWs is small when compared to thin films, strong luminescence is recorded in the whole temperature regime from 4 to 320 K, indicating the high crystal quality of the material. The emission energy remains constant for material investigated at different locations on the Ge substrate, illustrating the reliable growth of $Ge_{0.81}Sn_{0.19}$ nanostructures. The characteristics of the PL describe the formation of a direct band gap material. Moreover, the PL data illustrate the high crystal quality of the NW material prepared in this study, matching the optical properties of $Ge_{1-x}Sn_x$ films.

RESULTS AND DISCUSSION

The growth of $Ge_{1-x}Sn_x$ nanostructures has been realized in a two-step CVD approach. First, the Sn growth seeds are deposited by low-pressure CVD on single crystal Ge (111) substrates using $Sn(N(CH_3)_2)_2$ at substrate temperatures of 548−573 K. The *in situ* formation of the Sn growth seeds prevents oxidation that could be caused by a substrate transfer from separate growth chambers. Subsequently, the temperature is adjusted to the desired deposition conditions for the *tert*-butylgermane precursor as Ge source. Key to the successful formation of $Ge_{1-x}Sn_x$ NWs using Sn is a high supersaturation of the Ge-source to enable a high growth rate at low temperatures of 523−623 K. The high growth rate is important to prevent the degradation of the $Ge_{1-x}Sn_x$ by diffusion of metallic Sn through the crystal,[23] but causes the simultaneous formation of a parasitic Ge film that can be easily removed *via* reactive ion etching as described in literature.[43] A typical to view scanning electron microscopy (SEM) image reveals almost exclusively circular features and a small number of elongated structures formed off-axis, as shown in Figure 1a.

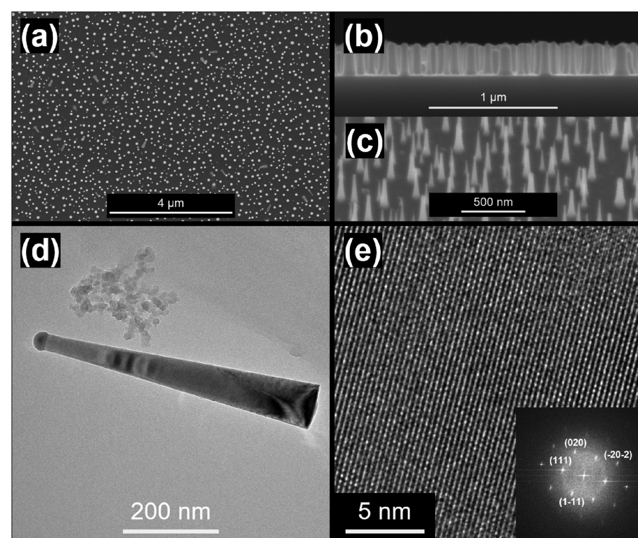

Figure 1. Top view (a) and cross section (b) of highly oriented $Ge_{1-x}Sn_x$ nanostructures grown on Ge (111) substrates at 598 K for 15 min and subsequent reactive ion etching. (c) The 30° tilted view shows fully terminated $Ge_{1-x}Sn_x$ NWs grown perpendicular to the Ge surface. (d) The TEM image of a NW scraped from the surface clearly illustrates the shrinking diameter due to the incorporation of Sn from the metallic hemispherical nucleation seed and smooth surface of the $Ge_{1-x}Sn_x$. (e) High-resolution TEM image of a $Ge_{1-x}Sn_x$ NW reveals the single crystalline nature of the material and the growth along the ⟨111⟩-axis, by the FFT shown in the inset.

The actual morphology of the NWs and their orientation can be visualized either in cross section geometry (Figure 1b) or simply by tilting the substrate off the ⟨111⟩-viewing direction, as demonstrated for fully terminated $Ge_{1-x}Sn_x$ NWs in Figure 1c. The highest yield of ⟨111⟩-oriented NWs (>97%) has been observed for samples where the bottom diameter of the grown NWs is in the range of 30−130 nm (mean value 81 ± 22 nm; 1σ), as illustrated in Figure S1. Transmission electron microscopy (TEM) is used to study microstructural properties of the $Ge_{1-x}Sn_x$ NWs. For that purpose, $Ge_{1-x}Sn_x$ NWs are deposited onto lacey carbon grids by drop casting of NWs which have been mechanically removed from the surface. The TEM image in Figure 1d reveals a smooth surface of the NW and shows the partially consumed hemispherical Sn growth seed with different diffraction contrast. The single crystal nature of the $Ge_{1-x}Sn_x$ material grown from the Sn seeds is shown by high-resolution TEM (Figure 1e). The fast Fourier

DOI: 10.1021/acsnano.9b02843
ACS Nano 2019, 13, 8047−8054

transformation (FFT) pattern in the inset depicts the growth direction of the $Ge_{1-x}Sn_x$ NW to be along the ⟨111⟩-axis, which can be expected given their perpendicular orientation to the Ge (111) substrate as illustrated in SEM images (Figure 1b).

Significant differences in morphology can be observed with higher amounts of Sn deposited in the first step. Thick micropillars of different height and diameter are obtained after the Ge deposition and accompanied by micron-sized structures migrating on the surface (Figure 2a). Micropillars are very similar to the structures observed in Figure 1b, but with a much larger diameter. The surface migrating in-plane micro/nanowires, as highlighted by cycles in Figure 2a, do not contain a significant Sn content (max. ~4 at%). Therefore, more details on the in-plane microwires are only provided in Figure S2 of the Supporting Information, since their composition observed in this study on Ge (111) single crystals is far from a desirable content of ~9 at% for a direct band gap material. The low Sn content in the in-plane micro/nanowires is very similar to the in-plane precipitates on Ge single crystals caused by Sn diffusion through $Ge_{1-x}Sn_x$ epilayers in the temperature range of 503−623 K.[44]

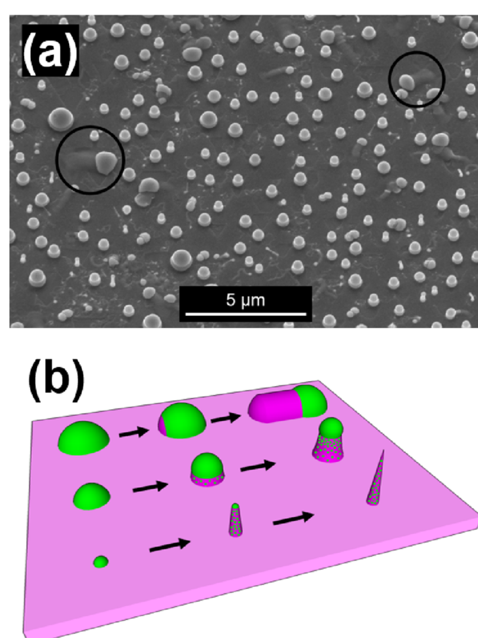

Figure 2. (a) SEM image (30° tilt angle) of structures obtained with a higher amount of Sn deposition showing in-plane growth of micro/nanowires and perpendicular growth of micropillars at growth temperatures of 573 K. Examples of in-plane microwires are circled to guide the eye. (b) A schematic illustration of the formation mechanism of the different structures obtained in this study including in-plane micro/nanowires and micropillars as well as the formation of NWs in the lower sequence.

A schematic diagram derived from SEM images can be used to discriminate between the three different morphologies observed in the experiments. The starting point in the growth description in Figure 2b is the size of the initial Sn particle. Small Sn particles lift from the surface of the Ge substrate easily, because the decomposing Ge can dissolve in the Sn particle leading to supersaturation with Ge and subsequent nucleation/film formation underneath the particle *via* layer-by-layer growth, representing a typical VLS growth of group IV NWs on (111)-oriented substrates of Si or Ge. The growth proceeds as long as the liquid Sn particle can facilitate the VLS growth of a single crystal, while the metal is consumed due to its incorporation in the growing $Ge_{1-x}Sn_x$ NWs. Increase in deposition duration for the Sn particles leads to larger base diameters owning large diameter distribution. In this scenario, either an identical $Ge_{1-x}Sn_x$ growth process perpendicular to the substrate surface occurs and micropillars are formed underneath the Sn particle or the nucleation event occurs at an edge of the particle at the triple phase boundary, resulting in in-plane migrating micro/nanowires.[45] Extending the micropillars has proven to be challenging, but higher temperatures and prolonged growth duration enable the formation of longer microwires. The as-grown microwires contain a thick Ge shell, but the core reveals a constant composition along their length (Figure S3). However, significant stability issues have been observed for the majority of the microwires leading to Sn segregation and secondary growth on the structures, as shown in Figure S4.

Since both thick micropillars and NWs are growing perpendicular to the Ge (111) substrate surface, the composition of the $Ge_{1-x}Sn_x$ material at the interface region to the Ge substrate has to be considered. For this purpose, TEM lamellae have been prepared using focused ion beam preparation methods for cutting and thinning of the sections. Figure 3a shows the composition at different locations along a scanning transmission electron microscopy-energy-dispersive X-ray (STEM-EDX) map of the micropillars, as illustrated in the inset. A clear trend is visible along the cross section starting at the Ge substrate and a gradient with increasing Sn content up to 15.4 at% over a length of 430 nm for a microwire of 1.1 μm base diameter. This is in good agreement with a recent study on epitaxial thin-film growth of $Ge_{1-x}Sn_x$ with a Sn content of ~15 at% at a distance of ~500 nm on a virtual Ge substrate.[46] In contrast, Figure 3b illustrates a NW with 95 nm base diameter owning a transition length of merely 50 nm for a 15 at% Sn content and 80 nm to reach a composition limit of ~19 at% Sn at the given synthesis temperature at 598 K. The composition along a NW after the initial transition zone is constant as shown in Figure 3c for a $Ge_{0.81}Sn_{0.19}$ NW (19.3 ± 0.9 at%) with the Sn particle at the growth front. The composition along a fully terminated NW is also constant, which is shown with the whole set of Ge and Sn maps and their overlays related to Figure 3 in Figures S6−S8. A deconvolution of the main parameter controlling the formation of this specific composition is not trivial. At a constant precursor ratio, a composition dependence in $Ge_{1-x}Sn_x$ on the growth temperature in thin-film samples was reported in literature for single layers[18] as well as multilayer grown by a step growth technique with associated sequential temperature decrease. In addition, these layers typically show constant composition after the strain effects are mostly compensated by a defective layer.[47,48] However, for NW growth, the influence of different catalyst/nucleation seeds altering the rate of crystal growth[20] as well as potentially changing precursor decomposition kinetics or efficiencies[49] have to be considered. High precursor concentration/vapor pressure relates to high supersaturation in the metal particle and thus a high chemical potential in the seed leading to high-growth rates during VLS growth, as reported for Au-assisted Si NW growth.[50] Moreover, the higher the PH_3 partial pressure, the higher the P doping level in Au-seeded Si NWs, illustrating the effect of the concentration of dopants in the seed particle on the

DOI: 10.1021/acsnano.9b02843
ACS Nano 2019, 13, 8047−8054

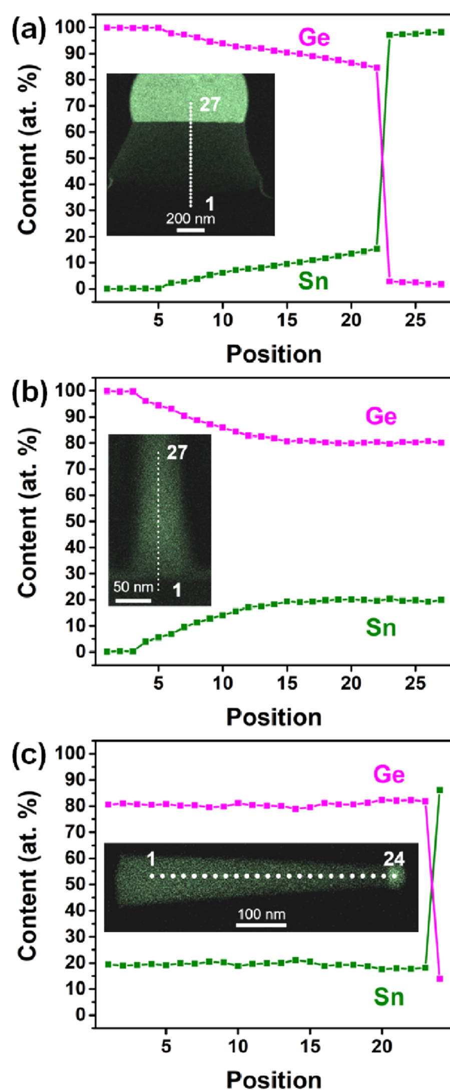

Figure 3. STEM-EDX maps showing the local Sn distribution in the $Ge_{1-x}Sn_x$ structures on the Ge substrate using thin TEM lamellae (a + b) prepared by FIB. Sn concentration profiles along the growth axis for (a) a micropillar with a base diameter of 1100 nm at the interface to the the Ge substrate showing a gradual increase of Sn composition over the whole length of the $Ge_{1-x}Sn_x$ segment and (b) the interface region between Ge and the growing $Ge_{1-x}Sn_x$ NW crystal with a base diameter of 95 nm, which reaches a constant Sn content (~19 at%) within a length of 80 nm. (c) The homogeneous Sn distribution along a $Ge_{1-x}Sn_x$ NW (19.3 ± 0.9 at %), which was mechanically removed from the substrate and transferred to the TEM grid.

material composition.[51] Thus, the incorporation of foreign atoms in a crystal lattice *via* the VLS growth also depends on the concentration of atoms in the growth promoter. Therefore, Sn self-seeding can be considered being an extreme, and the highest Sn content possible under the given growth parameters should be incorporated in the NW crystal. In addition, a diameter-independent composition is observed in the low diameter regime of our growth study, and thus a similar growth velocity can be assumed for the $Ge_{1-x}Sn_x$ growth. This assumption is based on the fact that the growth rate can influence the composition of group IV NWs dramatically with an increased incorporation efficiency of the metallic seed material in accelerated crystal growth of tens of nm per second.[52] The growth rate observed in this study on $Ge_{1-x}Sn_x$ NW formation is in the range of ~0.4 nm·s^{-1} and ~1 nm·s^{-1} for the growth of $Ge_{0.81}Sn_{0.19}$ NWs at 598 K, and no significant differences in composition could be observed. These values are in good agreement with reported growth rates for VLS-grown $Ge_{1-x}Sn_x$ NWs[19] and other group IV NW materials with high dopant incorporation efficiency.[51] At the here applied very high Ge precursor concentration/partial pressure range and low temperature during $Ge_{0.81}Sn_{0.19}$ growth, contributions of the Gibbs–Thomson effect are not expected to play a role in the last stages of the crystal termination.[53] However, the exact contributions of the individual factors described *vide supra* on the final composition of the $Ge_{1-x}Sn_x$ NWs will be evaluated in a separate study.

The partial substitution of Ge by Sn owning a 15% larger atomic size causes a lattice mismatch between the Ge substrate and the $Ge_{1-x}Sn_x$ alloy. Therefore, a diameter dependence on the transition zone in epitaxial growth of $Ge_{1-x}Sn_x$ micropillars or NWs on Ge substrates can be explained by the relief of strain which is counteracting the Sn incorporation. In epitaxial thin-film growth, this strain can relax either by defect formation or remains in compressively strained pseudomorphic films; however, both effects are affecting the optical properties of the material. The lattice mismatch is given by $\varepsilon = (a_f - a_s)/a_s$, where a_f and a_s are the lattice constants of the film and the substrate material, respectively. The lattice parameters of unstrained $Ge_{1-x}Sn_x$ scale linear with changes in the atomic ratio, and thus calculations of unit cell parameters according to Vegard's law can be used for the composition of interest. The transition zone from pure Ge to $Ge_{0.85}Sn_{0.15}$ with ε = 2.20% for a micropillar with a base diameter of 1.1 μm stretches 430 nm (Figure 3a), which is in good agreement with gradients observed in thin-film growth.[46,54] The similarities are caused by the large interface area of ~9.5 × 10^5 nm^2. In contrast, an identical composition is observed for the 95 nm diameter NW (interface area 7.0 × 10^3 nm^2) within 50 nm from the interface. The higher equilibrium composition of $Ge_{0.81}Sn_{0.19}$ with a nominal lattice mismatch of ε = 2.94% to the Ge substrate is reached after 80 nm, which relates to an effective strain compensation by dilatation. Since the substrate and the growing material are isomorphous, the strain can be gradually compensated. Such gradients are not possible for two materials with fixed composition and lattice parameters such as III–V semiconductors grown on group IV substrates. However, these literature reports demonstrate that NWs with small diameters can efficiently compensate a large amount of strain by dilatation, which is also observed here in the $Ge_{0.81}Sn_{0.19}$ NW growth with a very short transition zone.[55]

The optical properties have been investigated by PL. The high compositional uniformity of the Sn concentration in the $Ge_{0.81}Sn_{0.19}$ NWs over the full sample is shown by a positional PL measurement at 4 K in which a constant emission energy is observed (Figure 4a). Naturally, the PL intensity corresponds to the areal density of NWs (Figure S9). A positional invariance of emission energy with varying intensity also illustrates that the $Ge_{0.81}Sn_{0.19}$ nanostructure composition is only governed by crystal growth parameters and not by the Sn particle density. Temperature-dependent normalized PL spectra of the $Ge_{0.81}Sn_{0.19}$ NWs at an excitation density of 5.4 kW·cm^{-2} are illustrated in Figure 4b. The low-temperature PL spectrum exhibits a peak centered around 0.35 eV associated with the $Ge_{0.81}Sn_{0.19}$ nanostructure and a second peak centered around 0.55 eV. This high-energy feature is

DOI: 10.1021/acsnano.9b02843
ACS Nano 2019, 13, 8047–8054

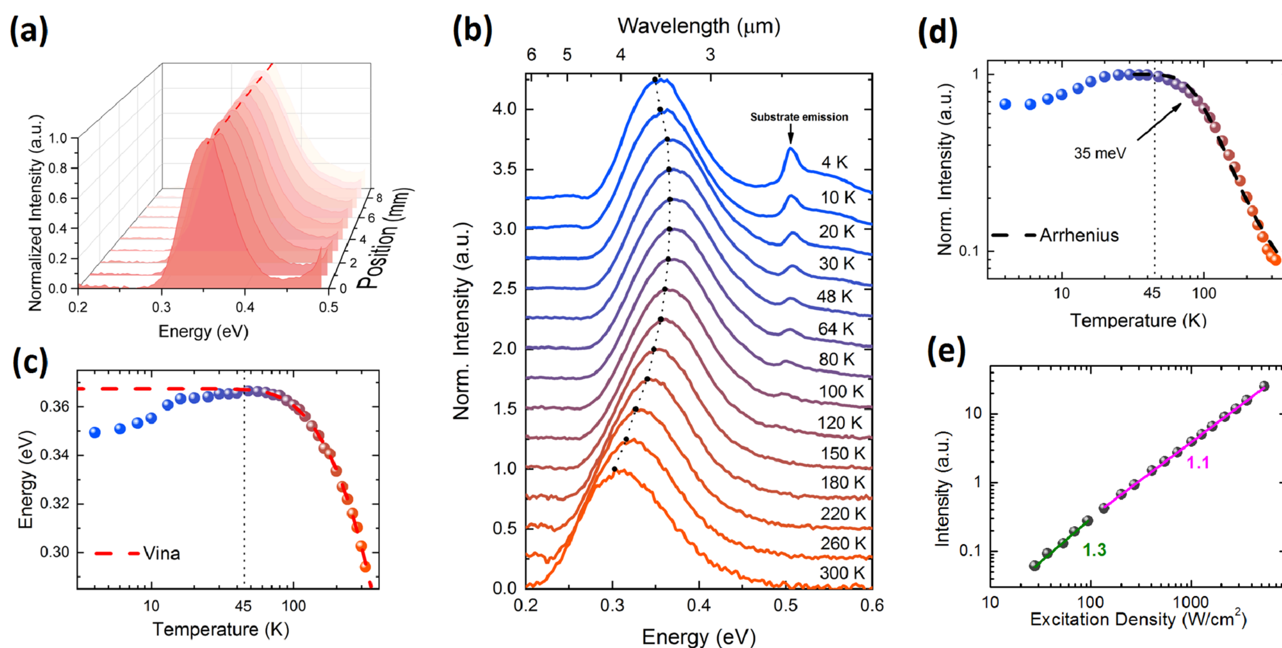

Figure 4. (a) The constant emission energy for different positions across a 10 × 10 mm substrate indicating the homogeneous Sn content of the $Ge_{0.81}Sn_{0.19}$ NWs over the whole sample. Spectra of the temperature dependence of the PL emission at an excitation density of 5.4 kW/cm^2 are plotted in (b) where the peaks of the spectra are indicated with a black dot. Further deconvolution results are illustrated in (c) where the peak energy is plotted. The measured data are well described with a Vina curve (ref 57). (d) The PL intensity as a function of temperature that is well fitted with a single exponential Arrhenius plot, while deviations are observed for low temperatures. (e) Log−log plot of the excitation density *versus* integrated PL intensity at different temperatures.

linked with luminescence centers in the antimony doped Ge substrates used in this study, as illustrated in Figure S10, and was not further investigated. For the temperature range from 4 K up to 45 K, the luminescence shifts from 0.35 eV to a higher energy of up to 0.37 eV and increases in intensity, as shown in Figure 4c,d. This behavior is commonly observed in $Ge_{1-x}Sn_x$ systems and is typically attributed to the detrapping of carriers from band gap-related localized states due to compositional fluctuations or defect states within the material.[39,56] The temperature-dependent emission energy shift occurs usually at 80−100 K, illustrating the excellent crystal quality observed in the material presented here. For temperatures higher than 45 K, the emission is caused by band-to-band recombination, and the emission energy upon temperature variation can be fitted using Vina's equation,[57] which is a suitable function to describe the band gap of Ge-like materials. Extrapolation of the model data to 4 K provides a low-temperature band gap of 0.37 eV. This result is in excellent agreement with the prediction of the band gap for unstrained $Ge_{0.81}Sn_{0.19}$.[42] The previous claim that the material is fully relaxed is further supported by the lack of observing a heavy-hole/light-hole splitting,[56,58] not even for low excitation densities as shown in Figure S11. The evolution of peak intensity in the temperature range of 4−320 K is illustrated in Figure 4d. For temperatures above 45 K, the intensity decays according to an Arrhenius function with a single exponential term and an activation energy of 37 meV. A monotonous decay of the intensity is a strong indication that the luminescence is due to direct band gap recombination.[8] To further understand the origin of the PL at low temperatures, an excitation density-dependent series was measured, as shown in Figure S9. The low-energy onset of the PL signals is independent of excitation density and marked with a dashed line at 0.28 eV, while the peak maximum shifts to higher energies by 33 meV when varying excitation density between 20 and 6000 W/cm^2. This suggests that we observe one or several band gap-related localized states that can be filled easily by increasing excitation power. A slope of $m \sim 1.1$ is observed for excitation densities above 100 W/cm^2, suggesting band-to-band recombination (Figure 4e). Similar behavior was also modeled for $Ge_{1-x}Sn_x$ layers in literature showing an analogous trend.[56] In general, the PL data presented here agree well with optical properties described for state of the art thin films[59,60] and demonstrate excellent optical characteristics for $Ge_{1-x}Sn_x$ semiconductor material formed in nanoscale dimensions by the here described approach. For instance, only a factor of 2 lower integrated PL intensity at 300 K is observed when compared to a thin-film sample containing 17.5 at% Sn,[59] while the excited $Ge_{1-x}Sn_x$ volume is <1/6 in the NW sample. This is a significant improvement when compared to literature on $Ge_{1-x}Sn_x$ NWs where a notable PL was merely observed at a low temperature of 80 K,[19] with exception of one report on Ge/GeSn core−shell NWs showing PL at room temperature.[39] Moreover, there are no reports on emission in the expected energy range for nanoparticles with varying $Ge_{1-x}Sn_x$ composition in the mid-IR range, but rather high-energy emissions close to values reported for Ge nanoparticles.[61,62]

CONCLUSION

In conclusion, we present a viable approach for the preparation of epitaxial $Ge_{1-x}Sn_x$ NWs with significant Sn incorporation (x up to ~0.19) on Ge(111) substrates. The compositional gradient from the pure Ge substrate to the final composition of the $Ge_{0.81}Sn_{0.19}$ NW material is confined to transition zones shorter than 100 nm, which is very narrow compared to transition zones for GeSn thin films. The growth relies on Sn seeds acting as a nucleation promoter as well as a source of the Sn component in the growing $Ge_{1-x}Sn_x$ crystal. Effects of the Sn particle size on the microstructure forming under the

DOI: 10.1021/acsnano.9b02843
ACS Nano 2019, 13, 8047−8054

applied growth conditions and the compositional evolution of structures grown perpendicular to the substrate have been evaluated. The optical properties reveal a typical and expected behavior of a direct band gap material when intensities of the PL signals are related to temperature as well as energy density input changes. The emission peak for the $Ge_{0.81}Sn_{0.19}$ NWs with an energy of ~0.3 eV at room temperature is in the mid-IR regime, and the absence of any sign of peak splitting illustrates that the structures are not strained. Moreover, the emission energy does not change upon varying the location on substrates, with peak intensity being naturally dependent on the density of $Ge_{0.81}Sn_{0.19}$ nanostructures. The optical properties in combination with the structural characterization illustrate the high crystal quality of the $Ge_{0.81}Sn_{0.19}$ material.

METHODS

All synthetic procedures and handling of the chemicals for the nanostructure synthesis have been carried out using Schlenk techniques or an argon-filled glovebox (MBraun). Solvents have been dried over sodium and stored in a glovebox. The bis(dimethylamido)tin(II) precursor ($Sn(N(CH_3)_2)_2$) was prepared by salt elimination using $SnCl_2$ and $Li(N(CH_3)_2)$ in dry hexane/diethyl ether according to literature.[63] The $Sn(N(CH_3)_2)_2$ was sublimed at reduced pressure before use. All chemicals for the synthesis of the amido precursor were purchased from Sigma-Aldrich. *tert*-Butylgermane (TBG; $(C_4H_9)GeH_3$) was purchased from Gelest.

Nanostructure Synthesis. Epitaxially grown $Ge_{1-x}Sn_x$ alloy nanostructures are synthesized in a cold-wall CVD reactor with glass and quartz tubes and fittings in the main reactor. A similar basic CVD assembly for one source has been described in literature.[64] In a typical process, the Ge (111) substrate is treated with concentrated hydrobromic acid (HBr) for 15 min in an ultrasonic bath to remove native oxides. Subsequently, the substrate is rinsed with distillated water and isopropyl alcohol. The dried substrate is connected to a graphite susceptor by silver paste. The CVD reactor is flushed with pure nitrogen for 15 min before separate 10 mL vessels containing finely ground 10 mg of bis(dimethylamido)tin ($Sn(N(CH_3)_2)_2$) and 50−200 μL TBG are attached to the growth chamber under nitrogen flow on separate lines with individual glass gauges. The CVD reactor is evacuated (~1×10^{-3} mbar) and dried under dynamic vacuum. The Sn deposition is carried out at substrate temperatures of 573 K and a temperature of 328 K of the oven containing the cold-wall reactor including the precursor vessels to generate sufficient vapor pressure of the metalorganic Sn precursor. After 10 min, the Sn precursor supply is disconnected and the susceptor temperature adjusted (523−623 K). At the desired susceptor temperature, the Ge precursor, which is a colorless liquid at room temperature with a very high vapor pressure, is frozen with liquid nitrogen. Cooling of the Ge source was carried out to increase the precursor concentration with a slight delay to account for the Sn particles incubation time before the NW growth starts. Since the Ge precursor thermally decomposes below the growth temperature, this procedure was used to offset the potential influences of a Ge layer formation on the substrates interfering with the nucleation of the NWs. A valve disconnecting the growth chamber from the vacuum system is closed before the valve to the Ge precursor is opened, and the previously condensed ^{t}Bu-GeH_3 is allowed to heat to room temperature. This procedure allows to achieve a high vapor pressure in the growth chamber during the decomposition of the Ge precursor (26−103 mbar calculated assuming ideal gas behavior and 298 K). The Ge precursor heats up to room temperature and thus filling the whole reaction vessel after ~40 s. Ge is deposited for 15 min, and the growth is terminated by opening the valve between the susceptor and the vacuum pump. The reactor is cooled down to room temperature after the reactor pressure is $<10^{-3}$ mbar.

After the CVD process, the substrates are transferred into a RIE etcher (Oxford Plasmalab 80 plus) to remove a parasitic, amorphous Ge layer grown on the substrate and the $Ge_{1-x}Sn_x$ structures. A mixture of 80% CF_4 and 20% O_2 is used as process gas. In a typical process, the samples are etched with an RF power of 35 W at a pressure of 700 mTorr. Depending on the expected thickness of the Ge layer, the etching time is varied between 30 and 75 s. The thin SnO_2 layer formed during the etching is removed by treatment in 10% HCl for 5 min. Dry etching using CF_4 and subsequent treatment with diluted HCl has been described in literature for the preparation of $Ge_{1-x}Sn_x$ microdiscs, and no influence on the optical properties was observed.[43]

Nanostructure Characterization. The $Ge_{1-x}Sn_x$ NWs were analyzed using a FEI Quanta 250 field emission gun scanning electron microscope (SEM). The $Ge_{1-x}Sn_x$ NWs were partially scraped off the Ge substrate and deposited on lacey carbon copper grids by drop casting of a toluene dispersion for transmission electron microscope (TEM) characterization (Plano). For cross sections, the structures were sputter-coated with carbon (100−500 nm), and Pt was deposited before FIB sectioning and thinning using a FEI-Quanta 200 3D DualBeam-FIB. In this study, a FEI TECNAI F20 operated at 200 kV and equipped with high-angle annular dark-field (HAADF) STEM and EDX detector was used. The elemental maps were recorded and quantified using the AMETEK TEAM package. The images were recorded and treated using Digital Micrograph software.

Optical Characterization. The samples have been illuminated using a 976 nm CW-diode laser, which was focused down to a spot of ~45 μm diameter onto the sample using an off-axis parabolic mirror. Using the same off-axis parabolic mirror, the PL was collimated and coupled into a Thermo Fischer IS50r FTIR equipped with an MCT detector and operated in step-scan mode. To filter out the thermal background, the laser was modulated at a frequency of ~35 kHz, which allowed the use of a lock-in technique. The samples were mounted in a helium-flow cryostat with heating for accurate temperature control, and the full setup was nitrogen purged to avoid any absorption peaks in the measured spectra. Examples for fitting the PL spectra are illustrated in Figure S12.

ASSOCIATED CONTENT

Supporting Information

The Supporting Information is available free of charge on the ACS Publications website at DOI: 10.1021/acsnano.9b02843.

Statistics on size of oriented NWs, additional STEM-EDX maps, SEM images, and PL data as well as examples for fitting operations (PDF)

AUTHOR INFORMATION

Corresponding Author

*E-mail: sven.barth@tuwien.ac.at; barth@physik.uni-frankfurt.de.

ORCID

Michael S. Seifner: 0000-0001-9101-5520
Johannes Bernardi: 0000-0002-4626-9246
Masiar Sistani: 0000-0001-5730-234X
Alois Lugstein: 0000-0001-5693-4775
Jos E. M. Haverkort: 0000-0003-3051-673X
Sven Barth: 0000-0003-3900-2487

Notes

The authors declare no competing financial interest.

ACKNOWLEDGMENTS

This work was funded by the Fonds zur Förderung der Wissenschaftlichen Forschung (FWF), Austria (project P 28524). Parts of this study were funded by the Deutsche Forschungsgemeinschaft (DFG, German Research Foundation), 413940754. A.D. has received funding from the

European Union's Horizon 2020 research and innovation program under grant agreement no. 735008.

REFERENCES

(1) Soref, R.; Buca, D.; Yu, S.-Q. Group IV Photonics: Driving Integrated Optoelectronics. *Opt. Photonics News* **2016**, *27*, 32−39.
(2) Mukherjee, S.; Assali, S.; Moutanabbir, O., Chapter Three - Group IV Nanowires for Carbon-Free Energy Conversion. In *Semiconductors and Semimetals*; Mokkapati, S., Jagadish, C., Eds. Academic Press: Cambridge, MA, 2018; Vol. *98*, pp 151−229.
(3) Oehme, M.; Kostecki, K.; Schmid, M.; Oliveira, F.; Kasper, E.; Schulze, J. Epitaxial Growth of Strained and Unstrained GeSn Alloys up to 25% Sn. *Thin Solid Films* **2014**, *557*, 169−172.
(4) Schulte-Braucks, C.; Glass, S.; Hofmann, E.; Stange, D.; von den Driesch, N.; Hartmann, J. M.; Ikonic, Z.; Zhao, Q. T.; Buca, D.; Mantl, S. Process Modules for GeSn Nanoelectronics with High Sn-Contents. *Solid-State Electron.* **2017**, *128*, 54−59.
(5) Ghetmiri, S. A.; Zhou, Y.; Margetis, J.; Al-Kabi, S.; Dou, W.; Mosleh, A.; Du, W.; Kuchuk, A.; Liu, J.; Sun, G.; Soref, R. A.; Tolle, J.; Naseem, H. A.; Li, B.; Mortazavi, M.; Yu, S.-Q. Study of a SiGeSn/GeSn/SiGeSn Structure Toward Direct Bandgap Type-I Quantum Well for all Group-IV Optoelectronics. *Opt. Lett.* **2017**, *42*, 387−390.
(6) Geiger, R.; Zabel, T.; Sigg, H. Group IV Direct Band Gap Photonics: Methods, Challenges, and Opportunities. *Front. Mater.* **2015**, *2*, 52.
(7) Olesinski, R. W.; Abbaschian, G. J. The Ge−Sn (Germanium−Tin) System. *Bull. Alloy Phase Diagrams* **1984**, *5*, 265−271.
(8) Wirths, S.; Geiger, R.; von den Driesch, N.; Mussler, G.; Stoica, T.; Mantl, S.; Ikonic, Z.; Luysberg, M.; Chiussi, S.; Hartmann, J. M.; Sigg, H.; Faist, J.; Buca, D.; Grützmacher, D. Lasing in Direct-Bandgap GeSn Alloy Grown on Si. *Nat. Photonics* **2015**, *9*, 88−92.
(9) Stange, D.; Wirths, S.; Geiger, R.; Schulte-Braucks, C.; Marzban, B.; von den Driesch, N.; Mussler, G.; Zabel, T.; Stoica, T.; Hartmann, J.-M.; Mantl, S.; Ikonic, Z.; Grützmacher, D.; Sigg, H.; Witzens, J.; Buca, D. Optically Pumped GeSn Microdisk Lasers on Si. *ACS Photonics* **2016**, *3*, 1279−1285.
(10) Al-Kabi, S.; Ghetmiri, S. A.; Margetis, J.; Pham, T.; Zhou, Y.; Dou, W.; Collier, B.; Quinde, R.; Du, W.; Mosleh, A.; Liu, J.; Sun, G.; Soref, R. A.; Tolle, J.; Li, B.; Mortazavi, M.; Naseem, H. A.; Yu, S.-Q. An Optically Pumped 2.5 μm GeSn Laser on Si Operating at 110 K. *Appl. Phys. Lett.* **2016**, *109*, 171105.
(11) Buca, D.; Von Den Driesch, N.; Stange, D.; Wirths, S.; Geiger, R.; Braucks, C. S.; Mantl, S.; Hartmann, J. M.; Ikonic, Z.; Witzens, J.; Sigg, H.; Grutzmacher, D.. GeSn Lasers for CMOS Integration. Proceedings from the *International Electron Devices Meeting (IEDM)*, December 2−6, 2017, San Francisco, CA; IEEE: New York, 2017; pp 22.3.1−22.3.4.
(12) Reboud, V.; Gassenq, A.; Pauc, N.; Aubin, J.; Milord, L.; Thai, Q. M.; Bertrand, M.; Guilloy, K.; Rouchon, D.; Rothman, J.; Zabel, T.; Pilon, F. A.; Sigg, H.; Chelnokov, A.; Hartmann, J. M.; Calvo, V. Optically Pumped GeSn Micro-Disks with 16% Sn Lasing at 3.1 μm up to 180 K. *Appl. Phys. Lett.* **2017**, *111*, No. 092101.
(13) Conley, B. R.; Margetis, J.; Du, W.; Tran, H.; Mosleh, A.; Ghetmiri, S. A.; Tolle, J.; Sun, G.; Soref, R.; Li, B.; Naseem, H. A.; Yu, S.-Q. Si Based GeSn Photoconductors with a 1.63 A/W Peak Responsivity and a 2.4 μm Long-Wavelength Cutoff. *Appl. Phys. Lett.* **2014**, *105*, 221117.
(14) Pham, T. N.; Du, W.; Conley, B. R.; Margetis, J.; Sun, G.; Soref, R. A.; Tolle, J.; Li, B.; Yu, S. Q. Si-Based $Ge_{0.9}Sn_{0.1}$ Photodetector with Peak Responsivity of 2.85 A/W and Longwave Cutoff at 2.4 μm. *Electron. Lett.* **2015**, *51*, 854−856.
(15) Tseng, H. H.; Wu, K. Y.; Li, H.; Mashanov, V.; Cheng, H. H.; Sun, G.; Soref, R. A. Mid-Infrared Electroluminescence From a Ge/$Ge_{0.922}Sn_{0.078}$/Ge Double Heterostructure *p-i-n* Diode on a Si Substrate. *Appl. Phys. Lett.* **2013**, *102*, 182106.
(16) Gupta, J. P.; Bhargava, N.; Kim, S.; Adam, T.; Kolodzey, J. Infrared Electroluminescence from GeSn Heterojunction Diodes Grown by Molecular Beam Epitaxy. *Appl. Phys. Lett.* **2013**, *102*, 251117.
(17) Chang, C.; Chang, T.-W.; Li, H.; Cheng, H. H.; Soref, R.; Sun, G.; Hendrickson, J. R. Room-Temperature 2-μm GeSn *p-i-n* Homojunction Light-Emitting Diode for In-Plane Coupling to Group-IV Waveguides. *Appl. Phys. Lett.* **2017**, *111*, 141105.
(18) von den Driesch, N.; Stange, D.; Wirths, S.; Mussler, G.; Holländer, B.; Ikonic, Z.; Hartmann, J. M.; Stoica, T.; Mantl, S.; Grützmacher, D.; Buca, D. Direct Bandgap Group IV Epitaxy on Si for Laser Applications. *Chem. Mater.* **2015**, *27*, 4693−4702.
(19) Biswas, S.; Doherty, J.; Saladukha, D.; Ramasse, Q.; Majumdar, D.; Upmanyu, M.; Singha, A.; Ochalski, T.; Morris, M. A.; Holmes, J. D. Non-Equilibrium Induction of Tin in Germanium: Towards Direct Bandgap $Ge_{1-x}Sn_x$ Nanowires. *Nat. Commun.* **2016**, *7*, 11405.
(20) Doherty, J.; Biswas, S.; Saladukha, D.; Ramasse, Q.; Bhattacharya, T. S.; Singha, A.; Ochalski, T. J.; Holmes, J. D. Influence of Growth Kinetics on Sn Incorporation in Direct Band Gap $Ge_{1-x}Sn_x$ Nanowires. *J. Mater. Chem. C* **2018**, *6*, 8738−8750.
(21) Seifner, M. S.; Biegger, F.; Lugstein, A.; Bernardi, J.; Barth, S. Microwave-Assisted $Ge_{1-x}Sn_x$ Nanowire Synthesis: Precursor Species and Growth Regimes. *Chem. Mater.* **2015**, *27*, 6125−6130.
(22) Barth, S.; Seifner, M. S.; Bernardi, J. Microwave-Assisted Solution-Liquid-Solid Growth of $Ge_{1-x}Sn_x$ Nanowires with High Tin Content. *Chem. Commun.* **2015**, *51*, 12282−12285.
(23) Seifner, M. S.; Hernandez, S.; Bernardi, J.; Romano-Rodriguez, A.; Barth, S. Pushing the Composition Limit of Anisotropic $Ge_{1-x}Sn_x$ Nanostructures and Determination of Their Thermal Stability. *Chem. Mater.* **2017**, *29*, 9802−9813.
(24) Sistani, M.; Seifner, M. S.; Bartmann, M. G.; Smoliner, J.; Lugstein, A.; Barth, S. Electrical Characterization and Examination of Temperature-Induced Degradation of Metastable $Ge_{0.81}Sn_{0.19}$ Nanowires. *Nanoscale* **2018**, *10*, 19443−19449.
(25) Seifner, M. S.; Sistani, M.; Porrati, F.; Di Prima, G.; Pertl, P.; Huth, M.; Lugstein, A.; Barth, S. Direct Synthesis of Hyperdoped Germanium Nanowires. *ACS Nano* **2018**, *12*, 1236−1241.
(26) Pertl, P.; Seifner, M. S.; Herzig, C.; Limbeck, A.; Sistani, M.; Lugstein, A.; Barth, S. Solution-Based Low-Temperature Synthesis of Germanium Nanorods and Nanowires. *Monatsh. Chem.* **2018**, *149*, 1315−1320.
(27) Acharya, S.; Ma, L.; Maldonado, S. Critical Factors in the Growth of Hyperdoped Germanium Microwires by Electrochemical Liquid−Liquid−Solid Method. *ACS Appl. Nano Mater.* **2018**, *1*, 5553−5561.
(28) Fahrenkrug, E.; Gu, J.; Jeon, S.; Veneman, P. A.; Goldman, R. S.; Maldonado, S. Room-Temperature Epitaxial Electrodeposition of Single-Crystalline Germanium Nanowires at the Wafer Scale from an Aqueous Solution. *Nano Lett.* **2014**, *14*, 847−852.
(29) Woo, R. L.; Gao, L.; Goel, N.; Hudait, M. K.; Wang, K. L.; Kodambaka, S.; Hicks, R. F. Kinetic Control of Self-Catalyzed Indium Phosphide Nanowires, Nanocones, and Nanopillars. *Nano Lett.* **2009**, *9*, 2207−2211.
(30) Fontcuberta i Morral, A.; Colombo, C.; Abstreiter, G.; Arbiol, J.; Morante, J. R. Nucleation Mechanism of Gallium-Assisted Molecular Beam Epitaxy Growth of Gallium Arsenide Nanowires. *Appl. Phys. Lett.* **2008**, *92*, No. 063112.
(31) Rathi, S. J.; Jariwala, B. N.; Beach, J. D.; Stradins, P.; Taylor, P. C.; Weng, X.; Ke, Y.; Redwing, J. M.; Agarwal, S.; Collins, R. T. Tin-Catalyzed Plasma-Assisted Growth of Silicon Nanowires. *J. Phys. Chem. C* **2011**, *115*, 3833−3839.
(32) Yu, L.; O'Donnell, B.; Alet, P.-J.; Conesa-Boj, S.; Peiró, F.; Arbiol, J.; Cabarrocas, P. R. i. Plasma-Enhanced Low Temperature Growth of Silicon Nanowires and Hierarchical Structures by Using Tin and Indium Catalysts. *Nanotechnology* **2009**, *20*, 225604.
(33) Mullane, E.; Kennedy, T.; Geaney, H.; Dickinson, C.; Ryan, K. M. Synthesis of Tin Catalyzed Silicon and Germanium Nanowires in a Solvent−Vapor System and Optimization of the Seed/Nanowire Interface for Dual Lithium Cycling. *Chem. Mater.* **2013**, *25*, 1816−1822.
(34) Lu, X.; Korgel, B. A. A Single-Step Reaction for Silicon and Germanium Nanorods. *Chem. - Eur. J.* **2014**, *20*, 5874−5879.

DOI: 10.1021/acsnano.9b02843
ACS Nano 2019, 13, 8047−8054

(35) Geaney, H.; Mullane, E.; Ramasse, Q. M.; Ryan, K. M. Atomically Abrupt Silicon−Germanium Axial Heterostructure Nanowires Synthesized in a Solvent Vapor Growth System. *Nano Lett.* **2013**, *13*, 1675−1680.
(36) Flynn, G.; Stokes, K.; Ryan, K. M. Low Temperature Solution Synthesis of Silicon, Germanium and Si−Ge Axial Heterostructures in Nanorod and Nanowire Form. *Chem. Commun.* **2018**, *54*, 5728−5731.
(37) Azrak, E.; Chen, W.; Moldovan, S.; Gao, S.; Duguay, S.; Pareige, P.; Roca i Cabarrocas, P. Growth of In-Plane $Ge_{1-x}Sn_x$ Nanowires with 22 at. % Sn Using a Solid−Liquid−Solid Mechanism. *J. Phys. Chem. C* **2018**, *122*, 26236−26242.
(38) Haffner, T.; Zeghouane, M.; Bassani, F.; Gentile, P.; Gassenq, A.; Chouchane, F.; Pauc, N.; Martinez, E.; Robin, E.; David, S.; Baron, T.; Salem, B. Growth of $Ge_{1-x}Sn_x$ Nanowires by Chemical Vapor Deposition *via* Vapor−Liquid−Solid Mechanism Using GeH_4 and $SnCl_4$. *Phys. Status Solidi A* **2018**, *215*, 1700743.
(39) Assali, S.; Dijkstra, A.; Li, A.; Koelling, S.; Verheijen, M. A.; Gagliano, L.; von den Driesch, N.; Buca, D.; Koenraad, P. M.; Haverkort, J. E. M.; Bakkers, E. P. A. M. Growth and Optical Properties of Direct Band Gap $Ge/Ge_{0.87}Sn_{0.13}$ Core/Shell Nanowire Arrays. *Nano Lett.* **2017**, *17*, 1538−1544.
(40) Meng, A. C.; Fenrich, C. S.; Braun, M. R.; McVittie, J. P.; Marshall, A. F.; Harris, J. S.; McIntyre, P. C. Core-Shell Germanium/Germanium−Tin Nanowires Exhibiting Room-Temperature Direct- and Indirect-Gap Photoluminescence. *Nano Lett.* **2016**, *16*, 7521−7529.
(41) Albani, M.; Assali, S.; Verheijen, M. A.; Koelling, S.; Bergamaschini, R.; Pezzoli, F.; Bakkers, E. P. A. M.; Miglio, L. Critical Strain for Sn Incorporation into Spontaneously Graded Ge/GeSn Core/Shell Nanowires. *Nanoscale* **2018**, *10*, 7250−7256.
(42) Attiaoui, A.; Moutanabbir, O. Indirect-to-Direct Band Gap Transition in Relaxed and Strained $Ge_{1-x-y}Si_xSn_y$ Ternary Alloys. *J. Appl. Phys.* **2014**, *116*, No. 063712.
(43) Gupta, S.; Chen, R.; Huang, Y.-C.; Kim, Y.; Sanchez, E.; Harris, J. S.; Saraswat, K. C. Highly Selective Dry Etching of Germanium over Germanium−Tin ($Ge_{1-x}Sn_x$): A Novel Route for $Ge_{1-x}Sn_x$ Nanostructure Fabrication. *Nano Lett.* **2013**, *13*, 3783−3790.
(44) Groiss, H.; Glaser, M.; Schatzl, M.; Brehm, M.; Gerthsen, D.; Roth, D.; Bauer, P.; Schäffler, F. Free-Running Sn Precipitates: an Efficient Phase Separation Mechanism for Metastable $Ge_{1-x}Sn_x$ Epilayers. *Sci. Rep.* **2017**, *7*, 16114.
(45) Wacaser, B. A.; Dick, K. A.; Johansson, J.; Borgström, M. T.; Deppert, K.; Samuelson, L. Preferential Interface Nucleation: An Expansion of the VLS Growth Mechanism for Nanowires. *Adv. Mater.* **2009**, *21*, 153−165.
(46) Assali, S.; Nicolas, J.; Moutanabbir, O. Enhanced Sn Incorporation in GeSn Epitaxial Semiconductors *via* Strain Relaxation. *J. Appl. Phys.* **2019**, *125*, No. 025304.
(47) Aubin, J.; Hartmann, J. M.; Gassenq, A.; Rouviere, J. L.; Robin, E.; Delaye, V.; Cooper, D.; Mollard, N.; Reboud, V.; Calvo, V. Growth and Structural Properties of Step-Graded, High Sn Content GeSn Layers on Ge. *Semicond. Sci. Technol.* **2017**, *32*, No. 094006.
(48) Margetis, J.; Yu, S.-Q.; Bhargava, N.; Li, B.; Du, W.; Tolle, J. Strain Engineering in Epitaxial $Ge_{1-x}Sn_x$: a Path Towards Low-Defect and High Sn-Content Layers. *Semicond. Sci. Technol.* **2017**, *32*, 124006.
(49) Borgstrom, M. T.; Immink, G.; Ketelaars, B.; Algra, R.; Bakkers, E. Synergetic Nanowire Growth. *Nat. Nanotechnol.* **2007**, *2*, 541−544.
(50) Pinion, C. W.; Nenon, D. P.; Christesen, J. D.; Cahoon, J. F. Identifying Crystallization- and Incorporation-Limited Regimes during Vapor−Liquid−Solid Growth of Si Nanowires. *ACS Nano* **2014**, *8*, 6081−6088.
(51) Christesen, J. D.; Pinion, C. W.; Zhang, X.; McBride, J. R.; Cahoon, J. F. Encoding Abrupt and Uniform Dopant Profiles in Vapor−Liquid−Solid Nanowires by Suppressing the Reservoir Effect of the Liquid Catalyst. *ACS Nano* **2014**, *8*, 11790−11798.
(52) Chen, W.; Yu, L.; Misra, S.; Fan, Z.; Pareige, P.; Patriarche, G.; Bouchoule, S.; Cabarrocas, P. R. i. Incorporation and Redistribution of Impurities into Silicon Nanowires During Metal-Particle-Assisted Growth. *Nat. Commun.* **2014**, *5*, 4134.
(53) Dayeh, S. A.; Picraux, S. T. Direct Observation of Nanoscale Size Effects in Ge Semiconductor Nanowire Growth. *Nano Lett.* **2010**, *10*, 4032−4039.
(54) Dou, W.; Benamara, M.; Mosleh, A.; Margetis, J.; Grant, P.; Zhou, Y.; Al-Kabi, S.; Du, W.; Tolle, J.; Li, B.; Mortazavi, M.; Yu, S.-Q. Investigation of GeSn Strain Relaxation and Spontaneous Composition Gradient for Low-Defect and High-Sn Alloy Growth. *Sci. Rep.* **2018**, *8*, 5640.
(55) Mårtensson, T.; Svensson, C. P. T.; Wacaser, B. A.; Larsson, M. W.; Seifert, W.; Deppert, K.; Gustafsson, A.; Wallenberg, L. R.; Samuelson, L. Epitaxial III−V Nanowires on Silicon. *Nano Lett.* **2004**, *4*, 1987−1990.
(56) Stange, D.; Wirths, S.; von den Driesch, N.; Mussler, G.; Stoica, T.; Ikonic, Z.; Hartmann, J. M.; Mantl, S.; Grützmacher, D.; Buca, D. Optical Transitions in Direct-Bandgap $Ge_{1-x}Sn_x$ Alloys. *ACS Photonics* **2015**, *2*, 1539−1545.
(57) Viña, L.; Logothetidis, S.; Cardona, M. Temperature Dependence of the Dielectric Function of Germanium. *Phys. Rev. B: Condens. Matter Mater. Phys.* **1984**, *30*, 1979−1991.
(58) Mączko, H. S.; Kudrawiec, R.; Gladysiewicz, M. Material Gain Engineering in GeSn/Ge Quantum Wells Integrated with an Si Platform. *Sci. Rep.* **2016**, *6*, 34082.
(59) Assali, S.; Nicolas, J.; Mukherjee, S.; Dijkstra, A.; Moutanabbir, O. Atomically Uniform Sn-Rich GeSn Semiconductors with 3.0−3.5 μm Room-Temperature Optical emission. *Appl. Phys. Lett.* **2018**, *112*, 251903.
(60) Wirths, S.; Buca, D.; Mantl, S. Si−Ge−Sn Alloys: From Growth to Applications. *Prog. Cryst. Growth Charact. Mater.* **2016**, *62*, 1−39.
(61) Tallapally, V.; Nakagawara, T. A.; Demchenko, D. O.; Özgür, Ü.; Arachchige, I. U. $Ge_{1-x}Sn_x$ Alloy Quantum Dots with Composition-Tunable Energy Gaps and Near-Infrared Photoluminescence. *Nanoscale* **2018**, *10*, 20296−20305.
(62) Alan Esteves, R. J.; Hafiz, S.; Demchenko, D. O.; Ozgur, U.; Arachchige, I. U. Ultra-Small $Ge_{1-x}Sn_x$ Quantum Dots with Visible Photoluminescence. *Chem. Commun.* **2016**, *52*, 11665−11668.
(63) Foley, P.; Zeldin, M. Bis(dimethylamido)tin(II). Synthesis and Characterization. *Inorg. Chem.* **1975**, *14*, 2264−2267.
(64) Mathur, S.; Barth, S.; Shen, H. Chemical Vapor Growth of $NiGa_2O_4$ Films: Advantages and Limitations of a Single Molecular Source. *Chem. Vap. Deposition* **2005**, *11*, 11−16.

DOI: 10.1021/acsnano.9b02843
ACS Nano 2019, 13, 8047−8054